RESEARCH ARTICLE

Figures and figure supplements

Hyperglycemia induced cathepsin L maturation linked to diabetic comorbidities and COVID-19 mortality

Qiong He and Miao-Miao Zhao *et al*.

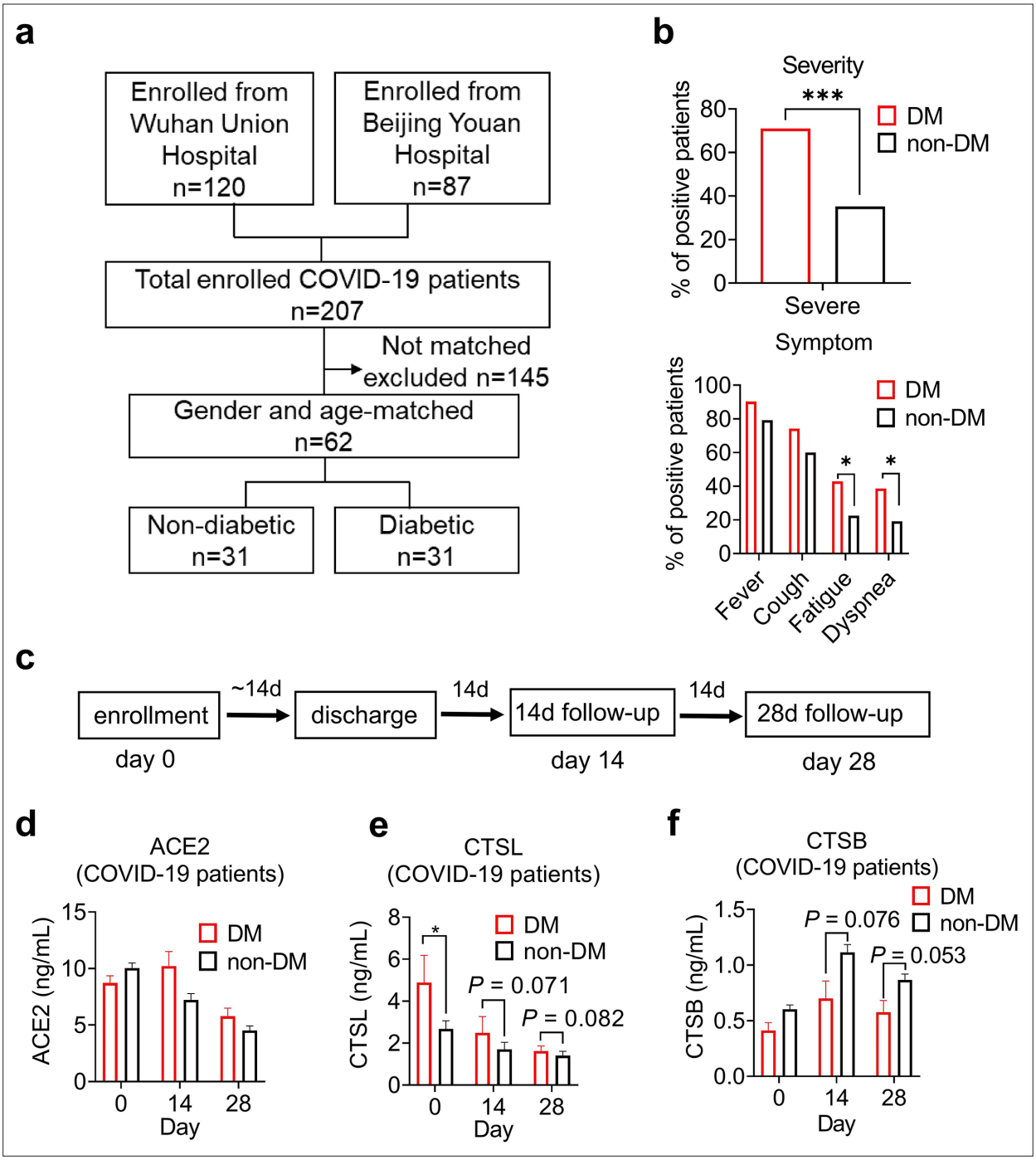

Figure 1. Disease severity and CTSL levels in COVID-19 patients with or without diabetes. (**a**) Design and inclusion flowchart of the case-control study. Out of 207 COVID-19 patients from two hospitals, 62 were included in the study after matching for gender and age, 31 with diabetes and 31 without. (**b**) Comparison of symptom severity and prevalence between diabetic and non-diabetic COVID-19 patients. (**c**) Study design and timeline of the enrollment and follow-up study. After admitted to the hospital (Day 0), patients were hospitalized for a mean duration of 14 days, followed up 14 days (Day 14) and 28 days (Day 28) after discharge, and blood samples were collected at each time point. (**d-f**) Plasma levels of COVID-19-related proteins were measured in diabetic and non-diabetic COVID-19 patients on Day 0, Day 14, and Day 28. Statistical significance was assessed by unpaired *t*-test (**b**) and Mann-Whitney *U*-test (**d-f**). The data are presented as the means ± SEM. *p<0.05, ***p<0.001.

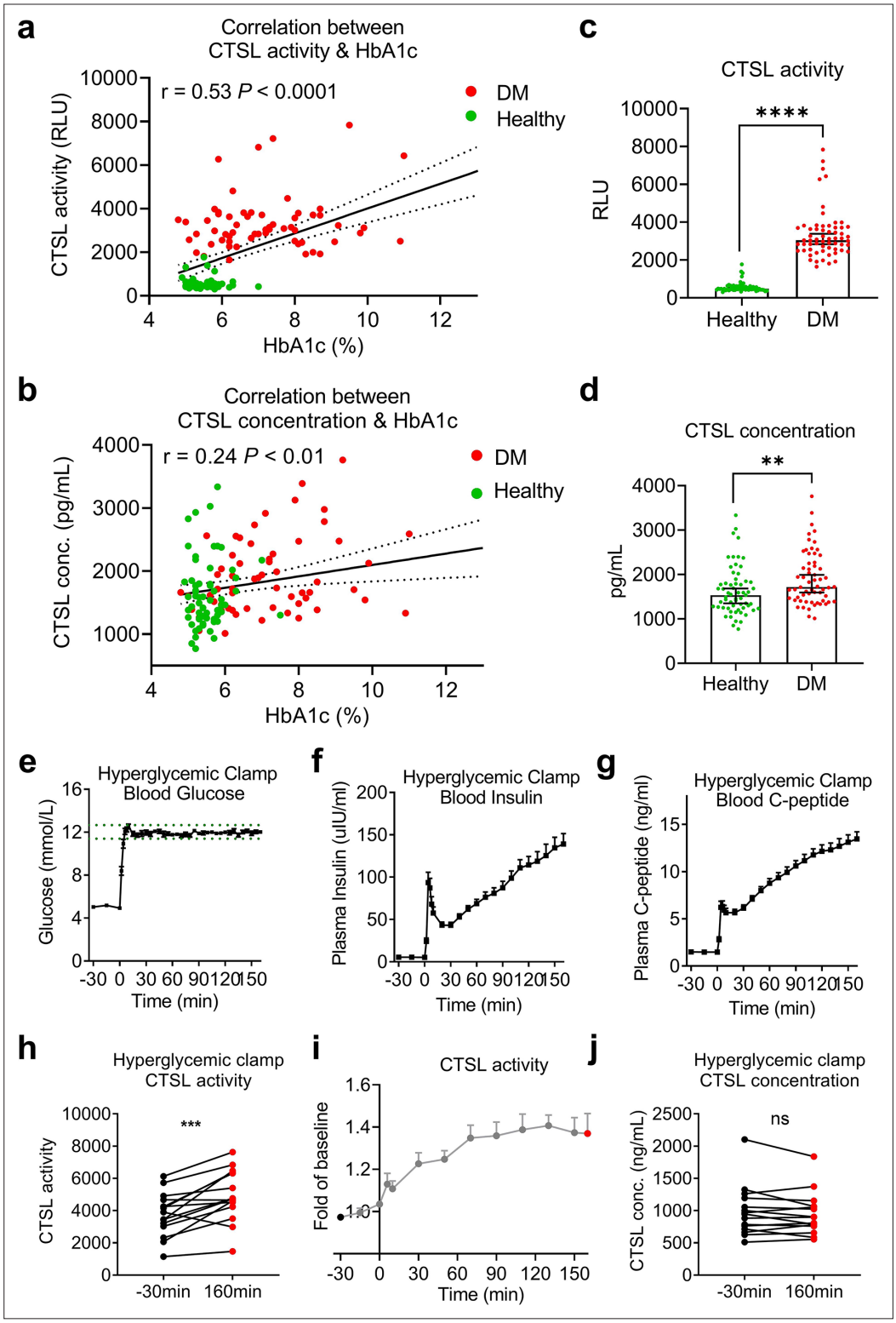

Figure 2. Impact of chronic and acute hyperglycemia on CTSL concentration and activity. (**a–d**) Effects of chronic hyperglycemia on CTSL activity and concentration in 122 gender- and age-matched individuals without COVID-19, including 61 euglycemic volunteers and 61 diabetic patients. (**a**) Correlation between plasma CTSL activity and blood glucose level indicated by HbA1c. (**b**) Correlation between plasma CTSL concentration and HbA1c. The dashed line represents the 95% CI in (**a and b**). (**c**) Comparison of plasma CTSL activity between the euglycemic and diabetic groups. (**d**) Comparison of plasma CTSL concentration between the euglycemic and diabetic groups.

Figure 2 continued on next page

Figure 2 continued

The data are presented as the median with 95% CI in (**c and d**). (**e-g**) Hyperglycemic clamp study performed in 15 healthy male subjects. (**e**) Plasma glucose levels in subjects throughout the clamp study. The dashed lines represent the range of ±5% of the hyperglycemic target level (basal blood glucose level +6.9 mmol/L). (**f**) Insulin levels and (**g**) proinsulin C-peptide levels throughout the clamp study. (**h–j**) Effects of acute hyperglycemia on CTSL concentration and activity in 15 healthy male volunteers. (**h**) Plasma CTSL activity at the beginning and the end of the clamp study. (**i**) Plasma CTSL activity throughout the clamp study. (**j**) Plasma CTSL concentration at the beginning and the end of the clamp study. Statistical significance was assessed by Spearman correlation analysis (**a and b**), unpaired *t*-test (**c and d**) and paired *t*-test (**h and j**). The data are presented as the means ± SEM. **p<0.01, ***p<0.001, ****p<0.0001.

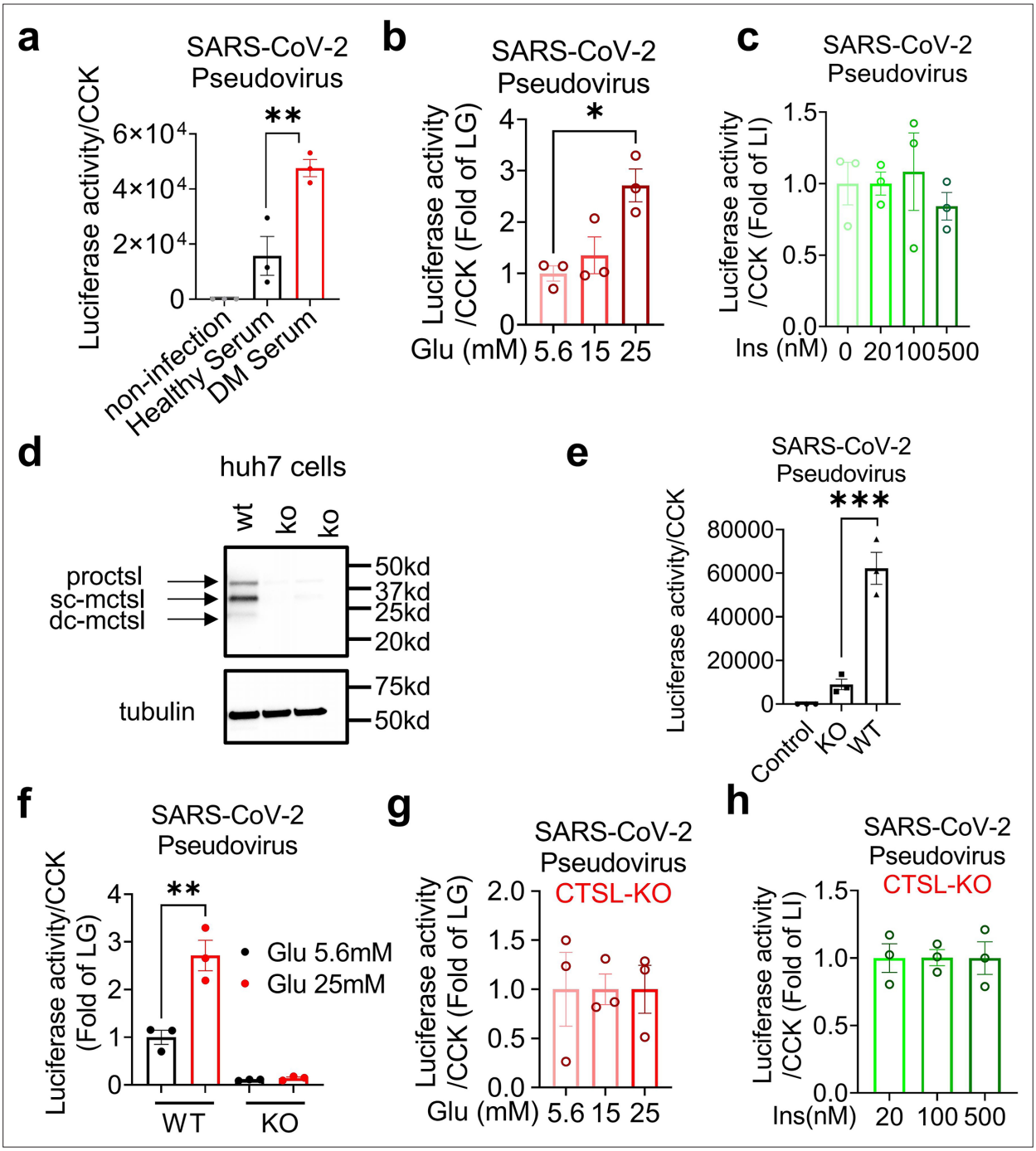

Figure 3. Hyperglycemia enhances SARS-CoV-2 infection through CTSL. Huh7 cells were infected with SARS-CoV-2 pseudovirus. (**a**) Wildtype (WT) cells cultured in sera from healthy and diabetic individuals were infected with SARS-CoV-2 pseudovirus (1.3×10^4 $TCID_{50}$/ml). Non-infected cells are used as control. The infection levels, as indicated by luciferase activities, were adjusted by cell viability, as indicated by CCK (n=3). (**b**) The SARS-CoV-2 infection rate of WT cells after being cultured in different doses of glucose (5.6 mM, 15 mM and 25 mM) (n=3). (**c**) The SARS-CoV-2 infection rate of WT cells after being cultured in different doses of insulin (0 nM, 20 nM, 100 nM and 500 nM) (n=3). (**d**) Comparison of CTSL expression in WT and *CTSL* knockout (KO) cell lines. (**e–h**) The SARS-CoV-2 pseudovirus infection of WT and *CTSL* KO cells. € The SARS-CoV-2 infection rate of control, *CTSL* KO, and WT cells (n=3). (**f**) The SARS-CoV-2 infection rate of WT and *CTSL* KO Huh7 cells cultured in different doses of glucose (5.6 mM and 25 mM) (n=3). (**g**) The SARS-CoV-2 infection rate of *CTSL* KO Huh7 cells cultured in different doses of glucose (5.6 mM, 15 mM and 25 mM) (n=3). (**h**) The SARS-CoV-2 infection rate of *CTSL* KO Huh7 cells cultured in different doses of insulin (20 nM, 100 nM and 500 nM) (n=3). Statistical significance was assessed by one-way ANOVA with Tukey's post hoc test (**a–c, e–h**). The data are presented as the means ± SEM. *p<0.05, **p<0.01, ***p<0.001.

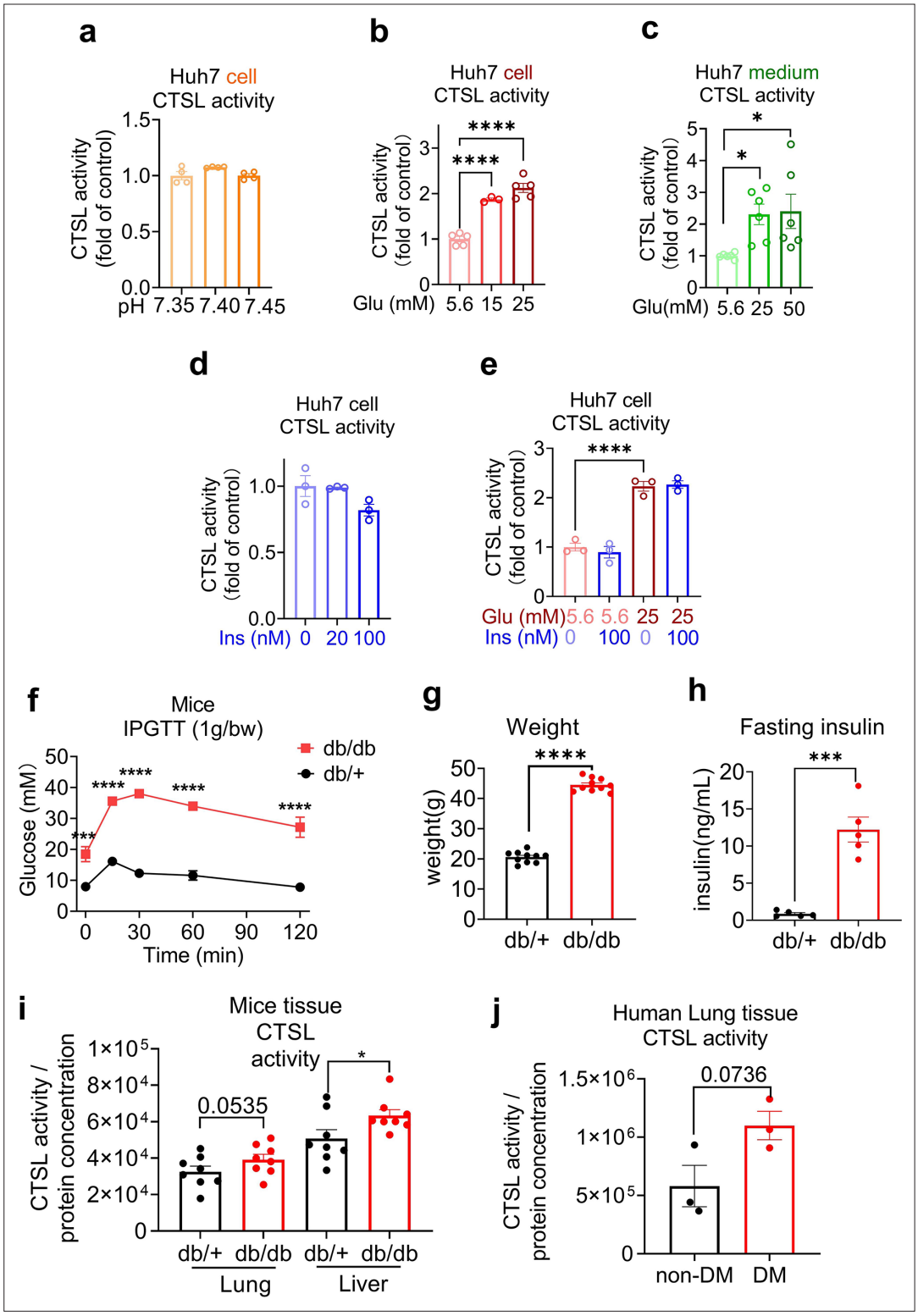

Figure 4. Elevation of glucose levels enhance CTSL activity. Effects of high glucose levels on CTSL activity in Huh7 cells, as well as in biopsy samples of mice and diabetic patients. (**a**) Intracellular CTSL activity was measured in Huh7 cells cultured in different pH as indicated (n=4). (**b**) Intracellular CTSL activity was measured in Huh7 cells cultured in different glucose concentrations as indicated (5.6 Glu group, n=5; 15 Glu group, n=3; 25 Glu group, n=5). (**c**) Extracellular CTSL activity was measured in Huh7 cells cultured in different glucose concentrations as indicated (n=6). (**d**) Intracellular CTSL activity was measured in Huh7 cells cultured in different insulin concentration

Figure 4 continued on next page

Figure 4 continued

as indicated (n=3). (**e**) Intracellular CTSL activity was measured in Huh7 cells cultured in different glucose and insulin concentrations as indicated (n=3). (**f**) Blood glucose levels during the intraperitoneal glucose tolerance test (IPGTT) in $Lepr^{db/db}$ mice and $Lepr^{db/+}$ mice (n=5). (**g**) Body weight of $Lepr^{db/db}$ mice and $Lepr^{db/+}$ mice was measured (n=10). (**h**) Fasting insulin levels were measured in $Lepr^{db/db}$ mice and $Lepr^{db/+}$ mice (n=5). (**i**) CTSL activity was measured in the lung and liver biopsy samples of $Lepr^{db/db}$ mice and $Lepr^{db/+}$ mice (n=8). (**j**) CTSL activity was measured in human lung biopsy samples from diabetic (DM) and non-diabetic patients (n=3). Statistical significance was assessed by one-way ANOVA with Tukey's post hoc test (**a–e**), two-way ANOVA with Sidak's multiple comparisons test (**f**) and unpaired *t*-test (**g–j**). The data are presented as the means ± SEM. *p<0.05, ***p<0.001, ****p<0.0001.

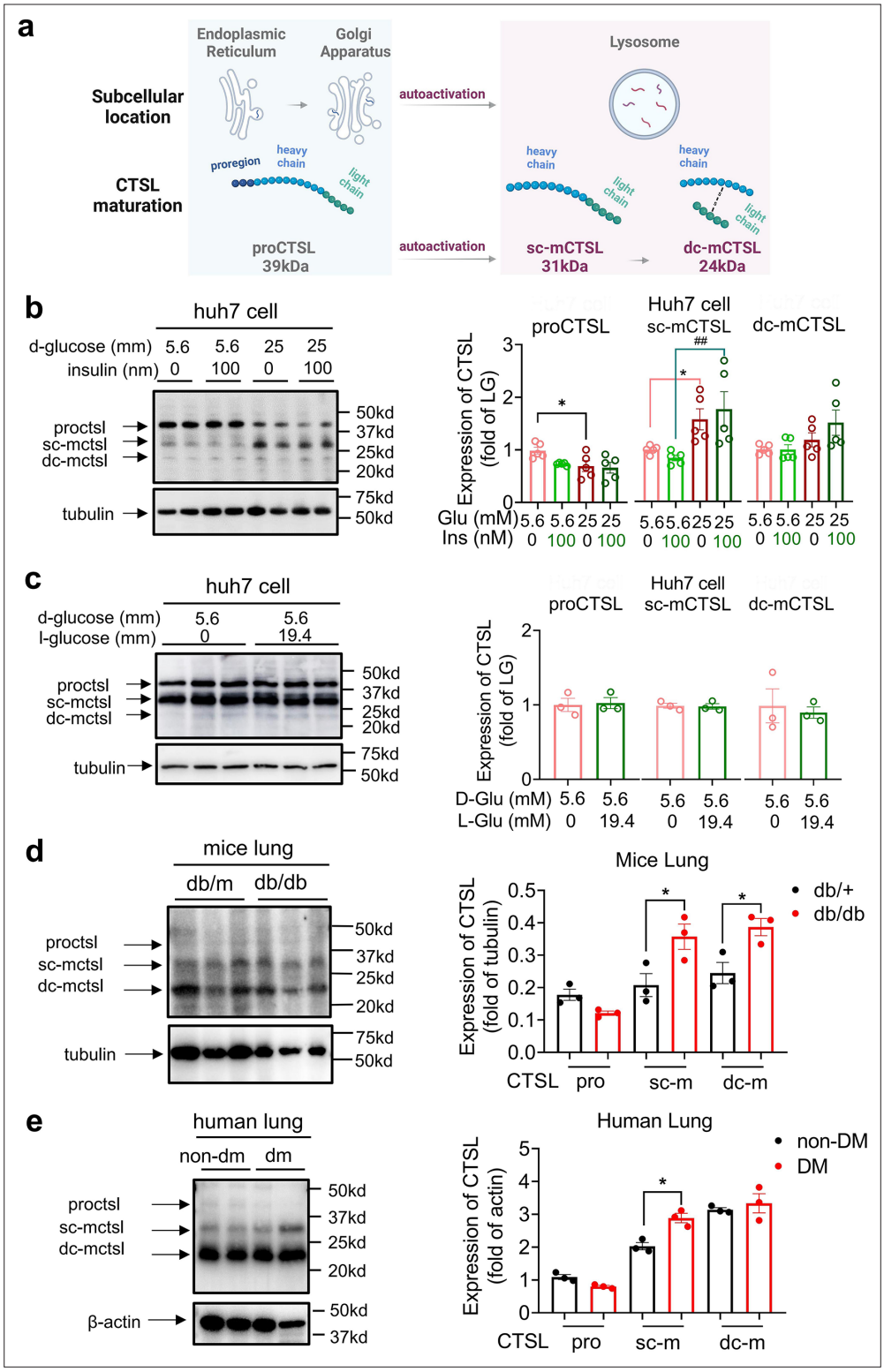

Figure 5. High glucose levels stimulate CTSL maturation. (**a**) Schematic of the CTSL maturation process. Pro-cathepsin L (ProCTSL, 39 kDa) in endoplasmic reticulum (ER) and Golgi apparatus translocated to the lysosome and autoactivated into the single chain mature cathepsin L (sc-mCTSL, 31 kDa) and double chain mature cathepsin L (dc-mCTSL, 24 KDa). (**b**) Western blot analysis of CTSL protein in Huh7 cells cultured with different doses of D-glucose and insulin as indicated (n=5). (**c**) Western blot analysis of CTSL protein in Huh7 cells cultured with 5.6 mM D-glucose or D-glucose plus 19.4 mM L-glucose as indicated (n=3). (**d**) Western blot analysis of CTSL protein in

Figure 5 continued on next page

Figure 5 continued

lung tissues from *Lepr*$^{db/db}$ mice and *Lepr*$^{db/+}$ mice (n=3). (**e**) Western blot analysis of CTSL protein in human lung tissues from non-diabetic and diabetic patients (n=3). Statistical significance was assessed by one-way ANOVA with Tukey's post hoc test (**b–e**). The data are presented as the means ± SEM. *p<0.05, $^{\#\#}$p<0.01.

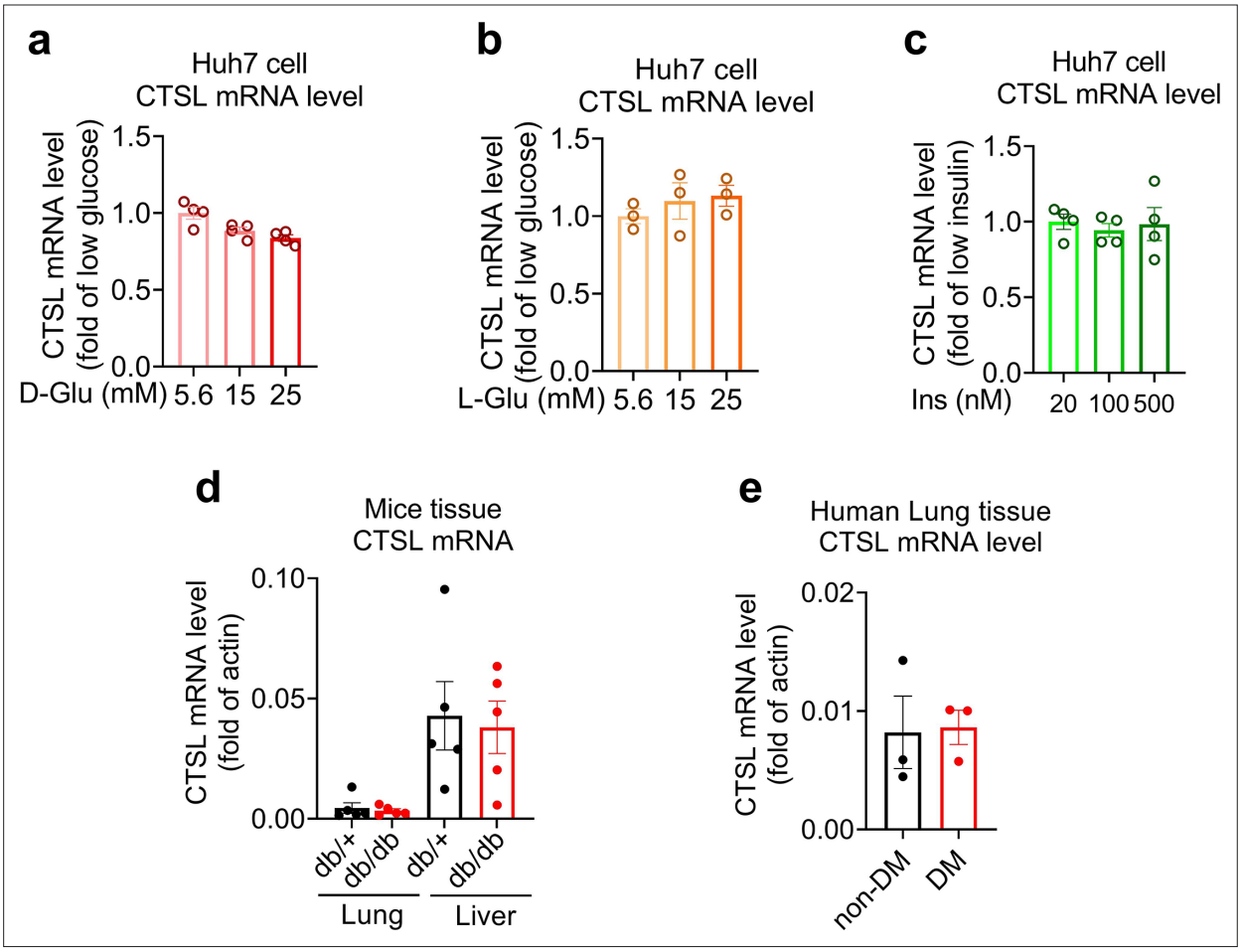

Figure 5—figure supplement 1. CTSL mRNA levels remain unchanged under different glucose conditions. (**a–c**) mRNA levels of CTSL in Huh7 cells cultured in media containing different concentrations of (**a**) D-glucose, (**b**) L-glucose, and (**c**) insulin, as indicated (n=3–4). (**d**) mRNA levels of CTSL in *Lepr*$^{db/db}$ mice and *Lepr*$^{db/+}$ mice lung and liver tissues (n=5). (**e**) mRNA levels of CTSL in human lung tissues (n=3). Significance was assessed by one-way ANOVA with Tukey's post hoc test (**a–c**) and Mann-Whitney *U*-test (**d and e**). The data are presented as the means ± SEM.

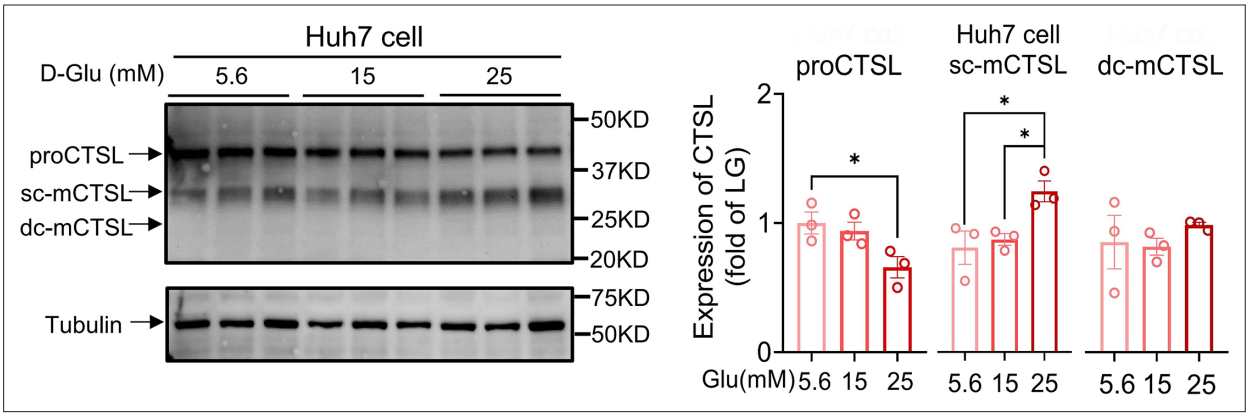

Figure 5—figure supplement 2. CTSL protein expression in Huh7 cells under different D-glucose concentrations. CTSL expression in Huh7 cells cultured in media containing different concentrations of D-glucose (n=3). Statistical significance was assessed by one-way ANOVA with Tukey's post hoc test. The data are presented as the means ± SEM. *p<0.05.

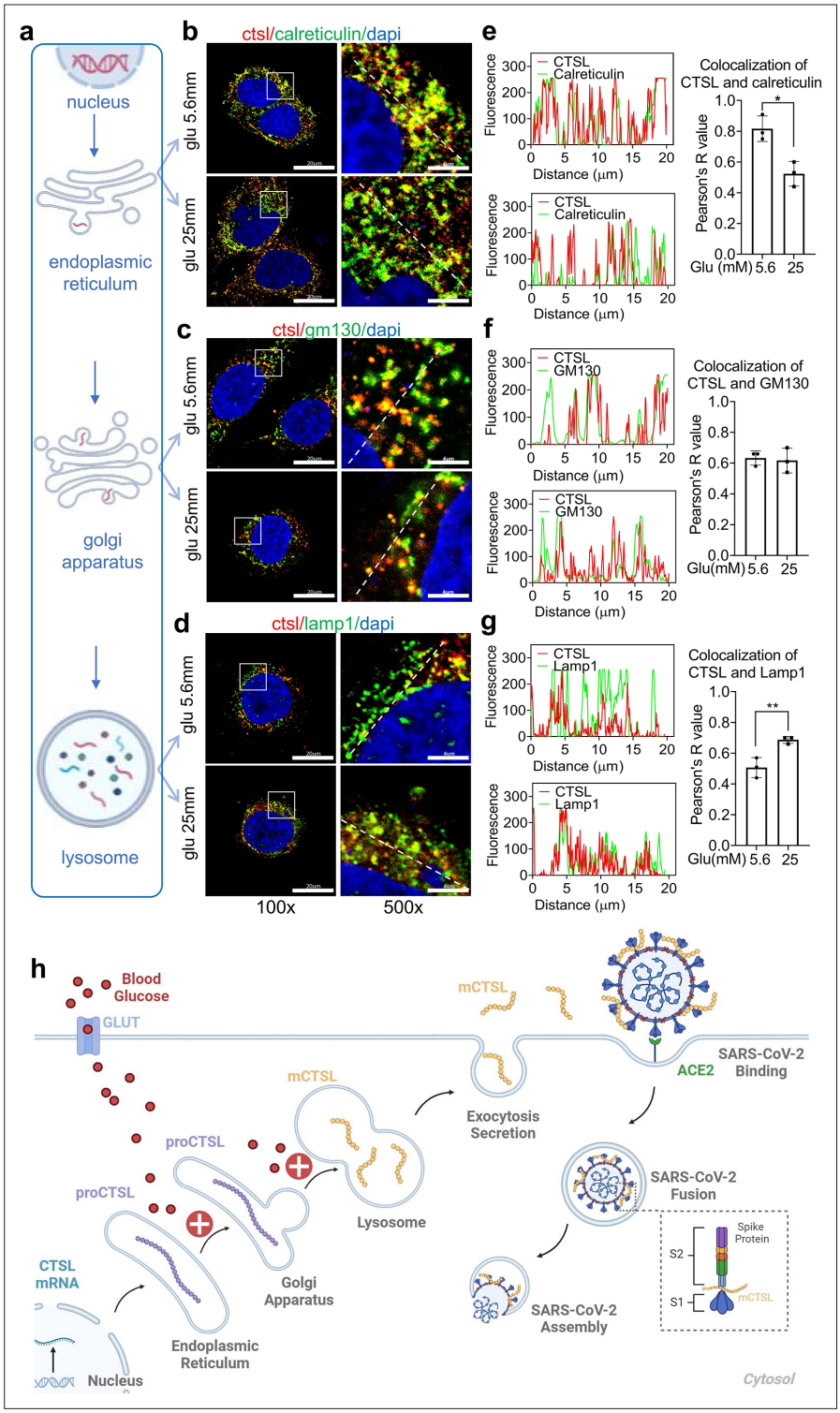

Figure 6. High glucose promotes CTSL translocation from endoplasmic reticulum to lysosome and enhances SARS-CoV-2 infection. (**a**) A diagram illustrating the process of CTSL translocation via the endoplasmic reticulum (ER)-Golgi-lysosome axis. (**b–d**) Immunofluorescent staining of Huh7 cells cultured in 5.6 mM or 25 mM glucose as indicated. Co-localization analysis of CTSL (labeled red) and different organelles (labeled green) was performed using CTSL and organelle marker protein antibodies. (**b**) calreticulin for ER, (**c**) GM130 for Golgi apparatus, and (**d**) lamp1 for lysosome. (**e–g**) Fluorescence co-localization intensity analysis of the dashed line on the 500 times enlarged immunofluorescence picture. Fluorescence co-localization intensity was calculated using the Plot

Figure 6 continued on next page

Figure 6 continued

Profile tool in Image J software (n=3). Scale bars, 20 μm for 100 x and 4 μm for 500 x. (**h**) Proposed mechanisms of hyperglycemia drives CTSL maturation and enhances SARS-CoV-2 infection. (1) Blood glucose increased in diabetic patients. (2) Hyperglycemia promoted CTSL maturation through the ER-Golgi-lysosome axis. (3) CTSL activity increased and facilitated SARS-CoV-2 entry, by cleaving the spike protein (consist of S1 and S2 subunits), and enhanced COVID-19 severity in diabetic patients. All statistical significance was assessed using unpaired *t*-test. The data are presented as the means ± SEM. *p<0.05, **p<0.01.

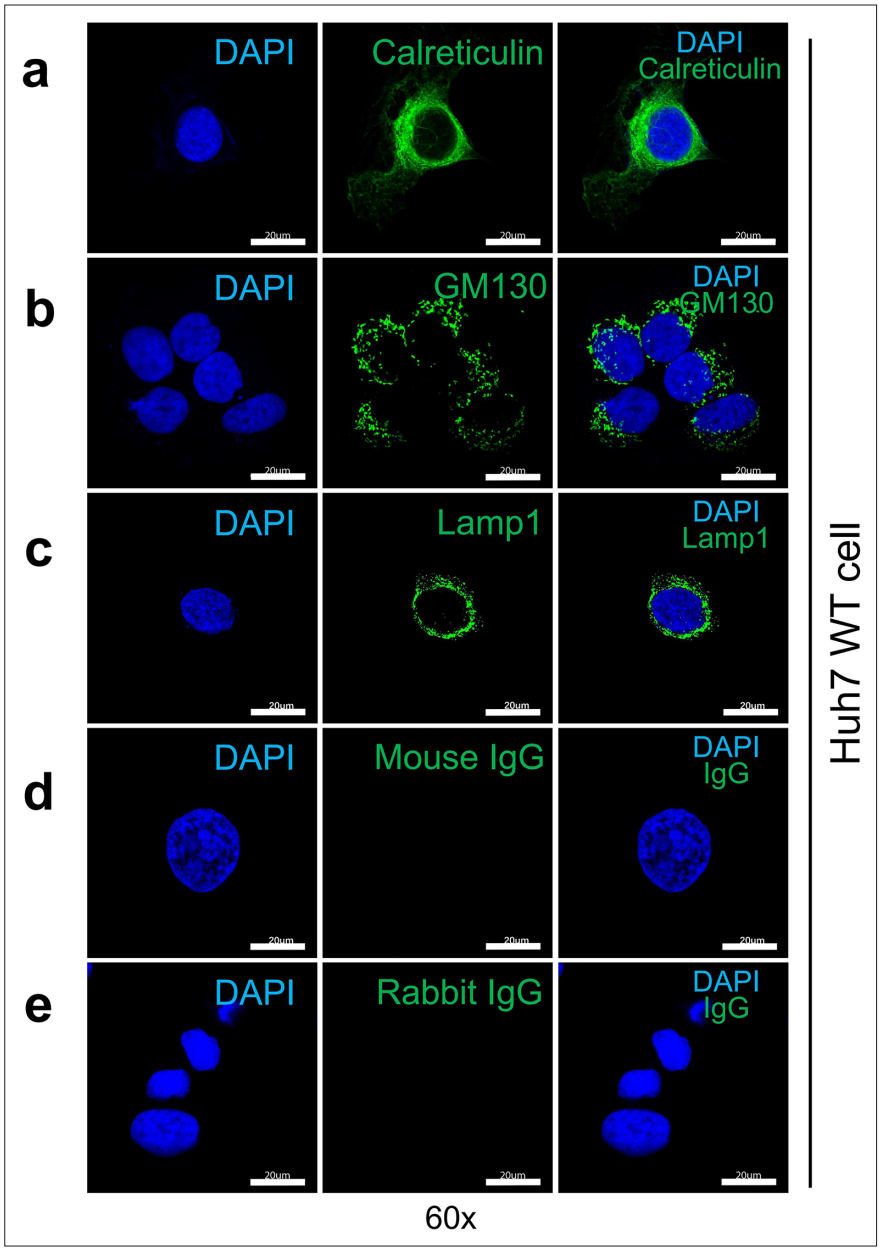

Figure 6—figure supplement 1. Immunofluorescent staining of organelle markers representing the endoplasmic reticulum (ER), Golgi apparatus and lysosome. (**a**) Expression of calreticulin (endoplasmic reticulum marker protein) in WT Huh7 cells. (**b**) Expression of GM130 (Golgi apparatus marker protein) in WT Huh7 cells. (**c**) Expression of Lamp1 (lysosome marker protein) in WT Huh7 cells. (**d**) Mouse immunoglobulin G (IgG) was used as a negative control to show the specificity of the primary antibody binding to GM130 and Lamp1 antigen. (**e**) Rabbit IgG was used as a negative control to show the specificity of the primary antibody binding to calreticulin antigen.

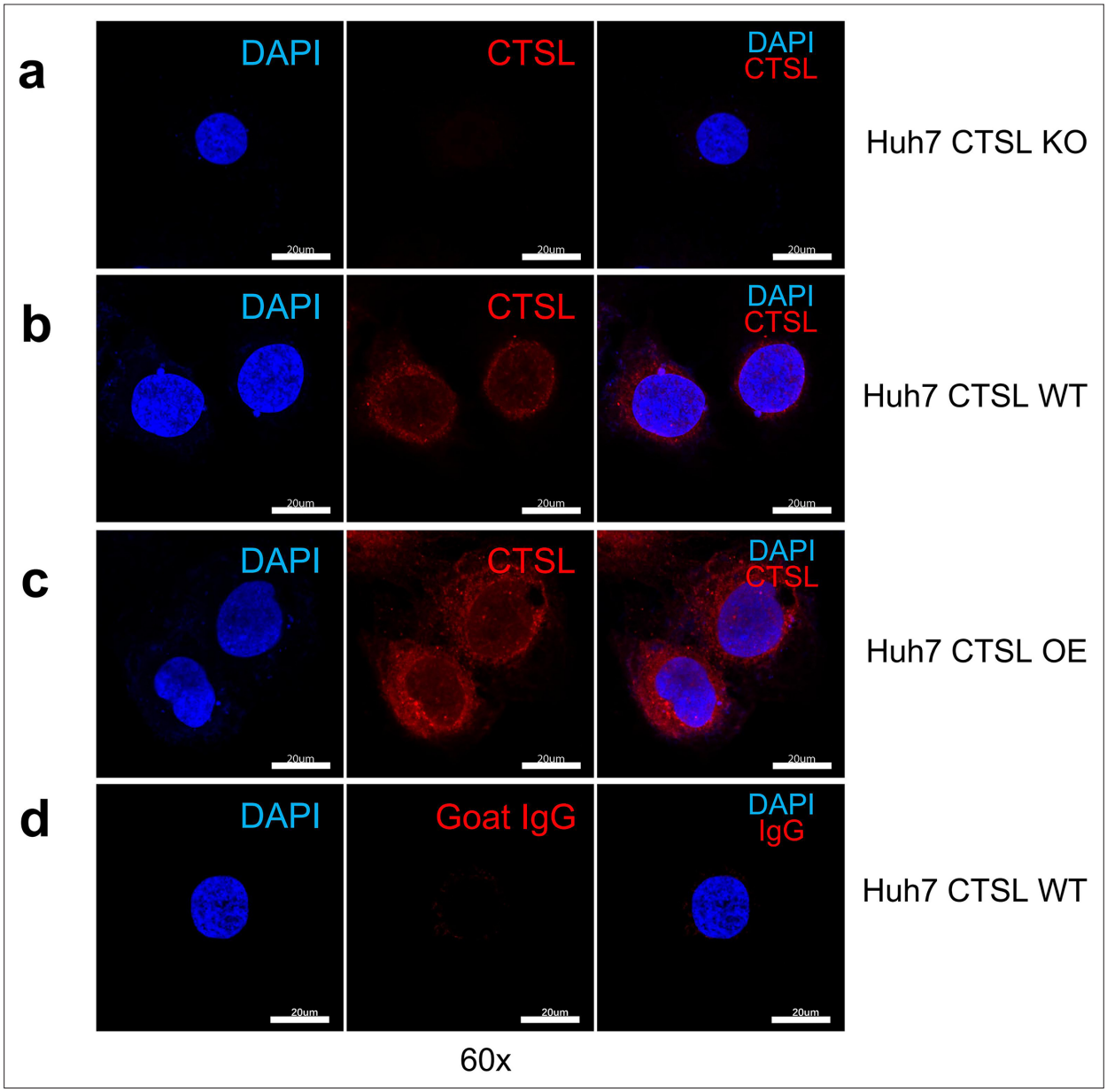

Figure 6—figure supplement 2. Immunofluorescent staining of CTSL in Huh7 cells. (**a**) CTSL expression in wild-type (WT) Huh7 cells. (**b**) CTSL expression in *CTSL* knockout (KO) Huh7 cells. (**c**) CTSL expression in overexpression (OE) Huh7 cells. (**d**) Goat IgG was used as a negative control to show the specificity of the primary antibody binding to CTSL antigen.